AIAA-RS5-2007-5004

Progress in Technology Demonstration for a Small Hybrid Launch Vehicle

John Tsohas[1], Lloyd J. Droppers[2], E. Glenn Case IV[3], Erik M. Dambach[4]
and Stephen D. Heister[5]
Purdue University, West Lafayette, IN, 47906

A hybrid rocket technology demonstrator is being developed and tested at Purdue University to serve as a test bed for flight testing technologies critical to the development of a small satellite launch vehicle. Consistent with this goal the demonstration vehicle will test subsystems such as hybrid propulsion, propellant feed systems, ground support equipment, recovery systems, thrust vector control, guidance, etc. Both 25 lbf and 250 lbf thrust hybrid rocket motors have been successfully hot-fire tested at the Purdue rocket test facilities. This paper details the progress made since the aforementioned hot-fire tests. The dual redundant recovery subsystem was successfully ground and flight tested using a solid motor booster, achieving an altitude of 4700 feet and reaching a maximum Mach number of 0.53. In addition, manufacturing and testing was completed on the ground support equipment used for remote loading and draining operations of hydrogen peroxide to and from the vehicle. Also under development is a 900 lbf thrust, multi-port, 90% hydrogen peroxide/ polyethylene hybrid rocket motor. This motor will be used to power the demonstration flight vehicle to altitudes exceeding 20,000 ft for flight testing of the thrust vector control subsystem at the NASA Wallops Flight Facility. A liquid injection thrust vector control (LITVC) subsystem creates side forces by injecting hydrogen peroxide in the supersonic portion of the nozzle and was chosen for our application. The LITVC subsystem currently under design will be hot-fire tested at Purdue rocket test facilities to obtain critical LITVC parameters such as side force and Isp data. In addition, guidance, navigation, and control software and hardware is being designed for use with the LITVC subsystem.

[1] Graduate PhD Student, School of Aeronautics and Astronautics, Purdue University.
[2] Graduate Masters Student, School of Aeronautics and Astronautics, Purdue University.
[3] Graduate Masters Student, School of Aeronautics and Astronautics, Purdue University.
[4] Graduate Masters Student, School of Aeronautics and Astronautics, Purdue University.
[5] Professor, School of Aeronautics and Astronautics, Purdue University.

INTRODUCTION

Purdue University School of Aeronautics and Astronautics is developing a hybrid rocket technology demonstrator to serve as a testbed for technologies critical to the development of a small satellite launch vehicle. A vehicle with the capability of placing a 10 lb payload in Low Earth Orbit could potentially serve to launch in-orbit flight experiments originating from both academia and industry. During the past 10 years, microsatellites in this weight class have shown great promise and use. One of the factors which hinder growth in the microsatellite industry is the considerable length of time it takes to secure a "piggy-back" ride into orbit on-board larger launch vehicles. Though the price for these secondary payloads is low, the queue for such launch opportunities can transverse several years. Quite often, secondary microsatellite payloads have to contend with an orbit pre-determined by the primary payload customer. A dedicated small launch vehicle would provide more launch opportunities and more desirable orbits for these small payloads.

The hybrid rocket technology demonstrator serves as a test-bed for technologies that will facilitate the design and development of the proposed small satellite launch vehicle. These critical technologies include propulsion, structures, separation, recovery, ground support, avionics and guidance, navigation and control sub-systems. These technologies will be demonstrated sequentially over a series of test flights. This will allow the designers to validate each of these sub-systems before adding more complexity, risk and features to the technology demonstrator.

Initially, a 25 lbf thrust hybrid rocket motor was designed, built and hot fire tested at the Purdue rocket propulsion facilities. Regression rate and performance data from these tests were used to design a larger, 250 lbf thrust, flight-weight hybrid rocket motor using 90% hydrogen peroxide (H_2O_2) and hydroxyl terminated polybutadiene (HTPB) propellants. Detailed information on the performance of the 25 and 250 lbf thrust motors can be found in Reference 4.

This paper details the progress made since the aforementioned hot fire tests. The first part of the paper details the development of a 900 lbf thrust hybrid rocket motor used for flight testing the thrust vector control system. The successful launch and recovery of the flight vehicle to validate the recovery sub-system is discussed next. In addition details on the manufacturing and testing of the ground support equipment are discussed. The final part of the paper discusses the design of the liquid injection thrust vector control (LITVC) sub-system to be hot-fire tested at the Purdue rocket test facilities.

PROGRESS ON THE TECHNOLOGY DEMONSTRATION FLIGHT VEHICLE

900 lbf THRUST HYBRID ROCKET MOTOR DESIGN AND HOT FIRE TESTING

Hybrid propulsion was chosen over liquid and solid propulsion due to cost, complexity and reliability constraints placed early in the design process[4]. More details on the trade studies performed and the reasoning for using hydrogen peroxide and hybrid propulsion can be found in Reference 4. Following the successful hot fire tests performed with the 250 lbf thrust, single-port, HTPB hybrid rocket motor in 2006, a more powerful 900 lbf thrust, 4-port, hybrid rocket motor was designed for use on other research endeavors as well as flight testing the demonstrator liquid injection thrust vector control (LITVC) system (see Fig. 1). The motor uses 90% hydrogen peroxide oxidizer and low density polyethylene (LDPE) fuel grain. The motor is a 4-port hybrid, a derivative of the earlier 250 lbf H_2O_2/HTPB single-port motor.

The 900 lbf thrust hybrid rocket motor was designed to operate at an average O/F ratio of 7.5 and an oxidizer mass flow rate of 3.6 lb/sec. The fuel ports were designed to provide oxidizer mass flux rate, G_{ox}, levels between 0.2-0.7 lb/in^2-s. Design chamber pressure was 400 psia MEOP and the fuel grain web thickness was designed to provide a minimum of 10 seconds of burn duration. The expansion nozzle was designed to be over-expanded at an exit pressure of 4.28 psia (A_e/A_t=11.7). Design parameters are presented in Table 1.

Thermochemical simulations ran using TEP[2] show that low density polyethylene (LDPE) offers comparable performance with HTPB fuel. In addition, the density of the two fuels is also comparable. For manufacturing a 4-port fuel grain, LDPE was preferred over HTPB due to its ease of manufacturing. For a 4-port fuel grain, HTPB would require a special assembly of 4 mandrels to be machined, in addition to mixing, curing and pouring of the HTPB inside the mold. After curing, the mold would have to be carefully pulled out of the hardened HTPB, making sure no tears are created during the process. On the other hand, LPDE was purchased in

the form of a solid rod, machined down to the desired outer diameter, and drilled to create the 4 ports.

The completed fuel grains are inserted inside an internal phenolic liner which acts as an insulator between the combustion gases and the external chamber walls, similar to the 250 lbf motor design. As shown in Fig. 1, the phenolic tube is inserted inside the combustion chamber designed to contain an internal pressure of 400 psia MEOP. A flanged connection is used to bolt the injector manifold assembly to the combustion chamber. To create a seal for the combustion gases, a butt-seal between the injector piece and the phenolic liner was designed. A secondary back-up seal is created by placing a silicon o-ring between the injector piece and the combustion chamber.

The nozzle uses ablative cooling and is manufactured from a monolithic silica phenolic billet, consisting of amorphous silica fibers in a phenol-formaldehyde phenolic resin matrix of proprietary formulation. This material has a density of ~1.80 gm/cm^3, and a thermal conductivity of ~0.20 BTU/ft-hr-F (at 500^{o}F). Sealing on the aft end of the motor is provided by a butt-seal between the phenolic liner and the ablative nozzle, similar to the seal design on the injector end. A secondary seal is created by a silicon o-ring placed between the nozzle o-ring groove and the chamber inner wall. The combustion chamber is designed with a recess in order to retain the nozzle in place and to provide positive pressure at the location of the butt-seal joint. Thermal protection of the injector face plate from combustion gases is accomplished by sheets of carbon-filled EPDM ablative insulation. In addition, high temperature RTV sealant is applied to the butt-seal joints for additional insulation and sealing. Also, the post combustion chamber is thermally protected with EPDM insulation and RTV sealant.

There are four stainless steel full cone spray injector nozzles mounted on the face plate. Each injector is sized to provide 0.9 lb/sec of oxidizer mass flow rate, with a pressure drop equal to 20% of average chamber pressure. The spray cone angle and nozzle orifice exit plane must be designed so that the oxidizer impinges on the inside of the star shaped surface of the consumable catalyst bed (CCB) ignition system. The CCB system previously invented at Purdue University causes hydrogen peroxide to decompose upon contact thus providing the necessary energy to initiate combustion of the H_2O_2/HTPB propellant combination. There are four CCBs located directly downstream of the injectors, mounted on the inner surface of the four LDPE fuel grain ports.

Designed solely for ground testing applications, the combustion chamber is manufactured from heavy steel pipe with welded flanges for attaching the oxidizer injector manifold. The injector manifold assembly consists of two stainless steel pieces which include mounts for the 4 injector nozzles, a manifold cavity for even propellant distribution, an oxidizer inlet port, recess for the butt-seal joint, and an o-ring groove for the secondary seal. The two pieces are bolted together to create the manifold cavity and sealing is provide by a Viton o-ring.

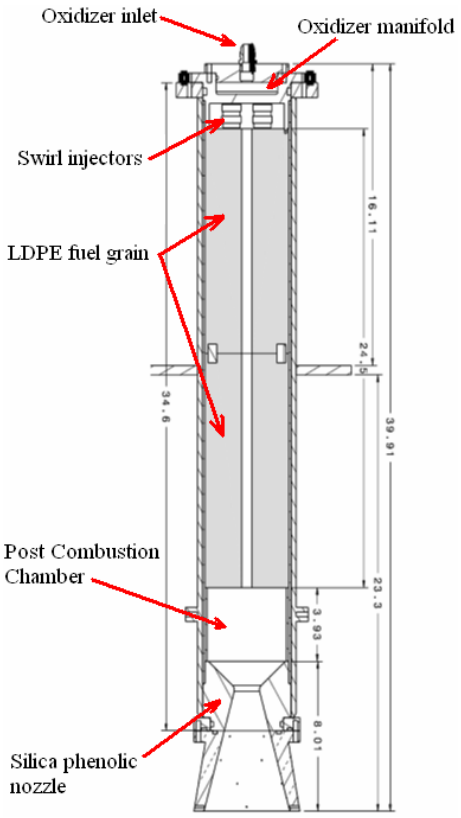

Figure 1. 900 lbf thrust hybrid rocket motor assembly drawing.

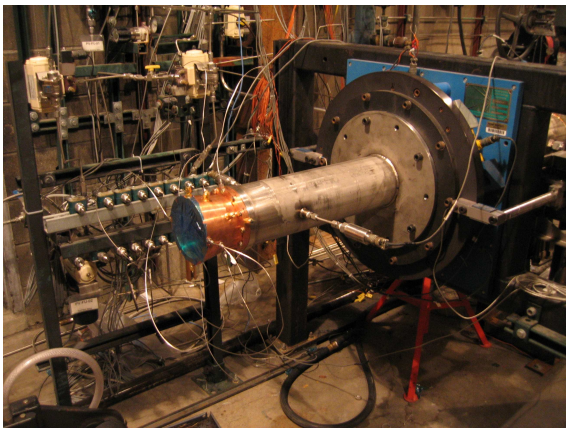

Figure 2. Picture of 900 lbf thrust hybrid rocket motor on test stand.

Table 1. 900 lbf thrust hybrid rocket motor design parameters

Chamber pressure:	400 psia
H2O2 flow rate:	3.6 lb/sec
Nominal thrust:	900 lbf
Burn time:	10 sec
Oxidizer:	90% H2O2
Fuel:	LDPE
Design O/F ratio:	7.5
Fuel grain length	24.5 in
CCB port depth:	6.2 in
Throat diameter	1.42 in
Nozzle area ratio	11.7
Nozzle cone angle	15 deg
Nozzle exit pressure	4.28 psia
Number of ports:	4

A series of hot fire tests were performed at the Purdue University rocket test facilities in order to verify the structural and thermal integrity of the injector face plate, post combustion chamber and nozzle, as well as to ensure no leakage was taking place past the primary and secondary seals. The tests aim to obtain fuel grain regression rate, performance, and nozzle ablation rate data for comparison with the hybrid rocket motor internal ballistics code. To date, a total of 3 hot fire tests have taken place with the 900 lbf thrust motor. The burn duration for the three tests was 5, 11.6 and 11.7 seconds respectively. All three hot-fire tests ran smoothly, with no signs of leakage past the primary or secondary seals, and minimal ablation of the carbon-filled EPDM insulation. No structural or thermal degradation was observed on the hardware. The silica phenolic ablation rate for the three tests averaged 5 mils/sec.

Fig. 4 shows the geometry of the 4-port LDPE fuel grain. Figs. 5 and 6 are before and after pictures of the fuel grain following an 11.6 sec burn. The results show even and axi-symmetric regression of the LDPE. Good test repeatability was observed as the regression pattern was similar for all three hot fire tests. The LDPE regression rate for the tests averaged 39 mils/sec. Fig. 7 shows the thrust profile of the first hot fire test.

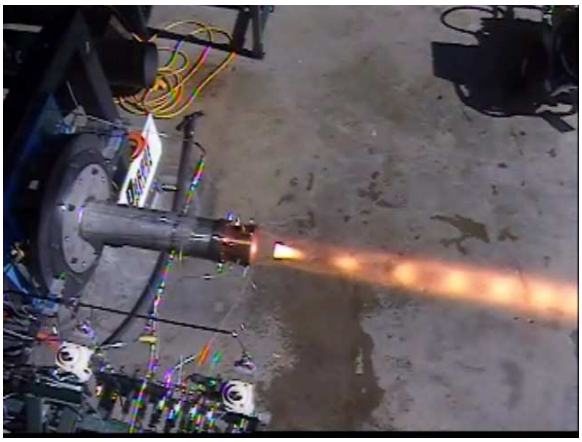

Figure 3. Picture of 900 lbf thrust hybrid motor hot fire test.

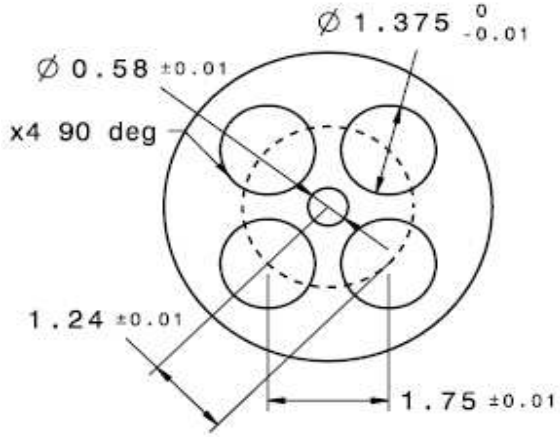

Figure 4. LDPE 4-port fuel grain design schematic.

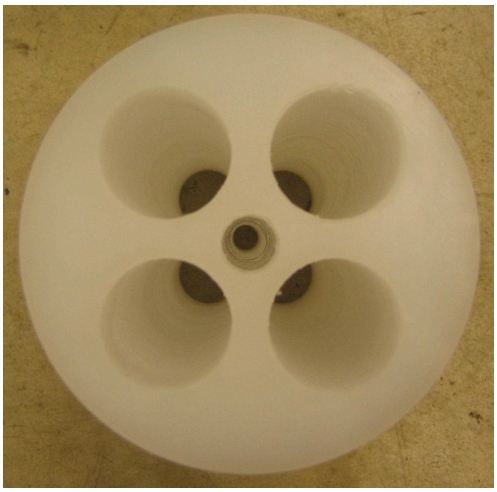

Figure 5. Picture of LDPE 4-port fuel grain before hot fire test.

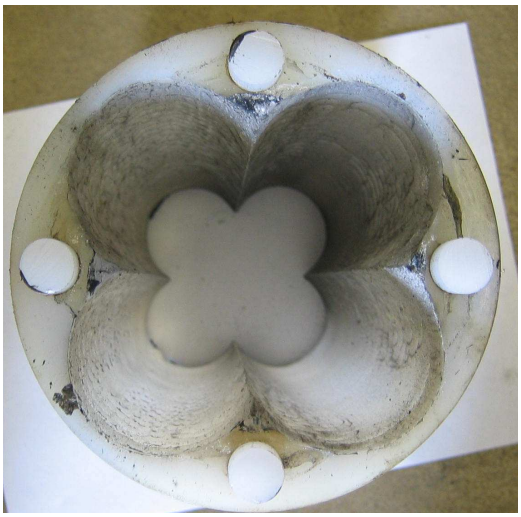

Figure 6. Picture of LDPE 4-port fuel grain after 11.6 second duration hot fire test.

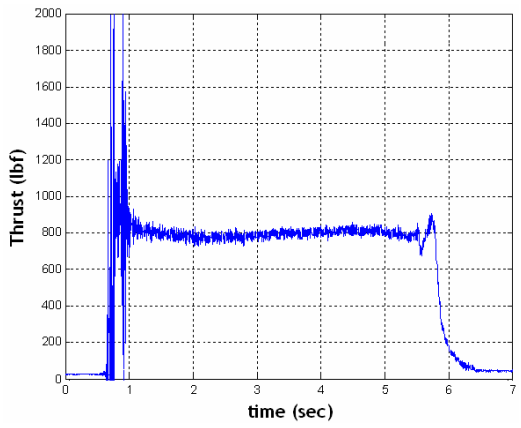

Figure 7. Thrust profile from 900 lbf motor hot fire test. Ambient pressure test, ε=11.7 (over-expanded nozzle).

FLIGHT-WEIGHT VERSION OF 900 lbf THRUST HYBRID ROCKET MOTOR

A flight weight version of the current 'ground test' article will be manufactured to power the demonstrator flight vehicle. Major design modifications include replacing the current carbon steel combustion chamber, stainless steel injector manifold and carbon steel flanges with high strength aluminum alloy, designed with minimum thickness to provide a structural safety factor of 2.0. The polyethylene fuel grain geometry will remain the same, while the injector manifold will be welded to the injector face to minimize mass. The nozzle will be modified by manufacturing a contoured silica phenolic nozzle, over wrapped with carbon-fiber in order to provide the required ablative material thickness for the lowest mass. The overall length and nozzle expansion ratio will remain the same. The aforementioned design modifications will reduce the 122 lb mass ground test motor to a 25 lb mass flight-weight version while keeping all the motor performance parameters the same. The ablative nozzle will incorporate the LITVC hardware and design which is detailed in the final section of this paper.

Table 2: Mass comparison between ground test and flight-weight versions of 900 lbf hybrid motor.

	Ground Test Version	Flight-weight Verison
Inert Mass (lb)	112.7	15.5
Propellant Mass (lb)	9.7	9.7
Total Mass (lb)	122.4	25.2

FLIGHT VEHICLE UPGRADES FOR 900 lbf PROPULSION

For the 900 lbf motor flights, the demonstration vehicle will upgrade its pressurization sub-system from previously used blow-down to a regulated pressure-fed design as shown in Fig. 8. As opposed to using only 25% of the propellant tank volume for oxidizer in the blow-down mode, with the addition of of a 4500 psia helium pressurant tank and a pressure regulator the pressure-fed design will allow 95% propellant tank volume utilization. This system will provide constant oxidizer feed pressure over the course of the burn, as well as a more efficient oxidizer tank utilization.

However, the increased performance of the pressure-fed system comes with an increase in overall system complexity. While the blow-down system employs one temperature measurement, one pressure

measurement, two solenoid valves, and one pressure relief valve, the pressure regulated system makes use of one temperature measurement, two pressure measurements, three valves, one pressure relief valve, one regulator, two burst disks and one pressurant tank. The helium pressurant tank will be designed for a maximum operating pressure of 4500 psia and will be manufactured from carbon-fiber material at the Purdue propulsion facilities.

The main oxidizer solenoid valve will be replaced with a burst disk, allowing for system simplicity, reduced weight and increased robustness. The pressure-fed system will require two ¼" gas solenoid valves operating at 600 psia, and one gas solenoid valve operating at 4500 psia as shown in Fig. 8. Two external quick disconnect umbilical lines will supply nitrogen and hydrogen peroxide to the flight vehicle. A new oxidizer pressure vessel is being designed with a new aluminum alloy to replace the existing tank. The tank will incorporate hemispherical end-caps and integral fuselage mounts in order to reduce weight.

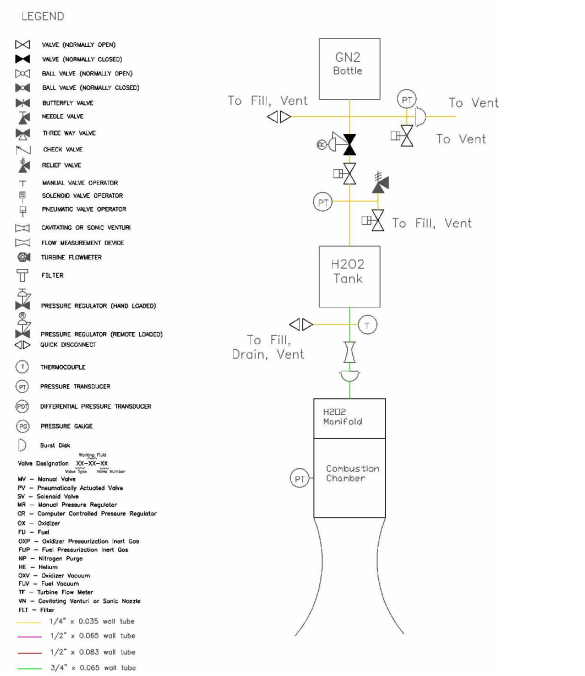

Figure 8. Plumbing and Instrumentation Diagram of flight-weight 900 lbf thrust hybrid rocket motor.

GROUND SUPPORT EQUIPMENT

The ground support equipment (GSE) is used for controlling the remote loading and draining of hydrogen peroxide to and from the flight vehicle. Assembly and construction of the GSE was completed in 2006 and was subjected to water and hydrogen peroxide tests in 2007. Currently the system consists of five ½" H2O2 compatible pneumatically actuated ball valves, 2 dome loaded manual pressure regulators, 2 pressure relief valves, 4 pressure transducers, 2 thermocouples, 4 check valves and associated ¼" pneumatic and ½"oxidizer lines as shown in Fig. A.1 in the appendix. Nitrogen is used to pressurize a hydrogen peroxide tank to the desired 600 psia ullage pressure in order to feed liquid oxidizer through a series of ball valves and into the flight vehicle propellant tank. Once propellant has been transferred onto the vehicle, nitrogen is supplied for the blow-down pressurization through the same oxidizer fill line (see Fig. A.1). The oxidizer fill line is disengaged from the vehicle by a remotely actuated quick-disconnect valve. To ensure safe launch operations, the oxidizer tank pressure and temperature are constantly monitored to verify that the hydrogen peroxide is not undergoing unexpected decomposition.

Launch is initiated by opening a normally closed, ½" on-board solenoid valve which allows hydrogen peroxide to flow into the hybrid motor combustion chamber. Spontaneous ignition and decomposition between the hydrogen peroxide and a consumable catalyst bed (CCB) located downstream of the injector, provides the needed energy to initiate combustion between the H2O2 and the HTPB fuel grain. In the event of an abort, the GSE has the capability of remotely draining the hydrogen peroxide into a dump tank located on the ground, by closing off the pressurization source, and opening the ½" dump valve. To ensure safety in launch operations, all circuits of the GSE and launch vehicle are designed to be fail-safe. In the event of an unexpected power outage, all solenoid valves return to their normal positions (normally open or closed) to allow venting of the tanks and automatic draining of the oxidizer from the launch vehicle directly into the dump tank. National Instruments Labview software is used for valve control and for monitoring system pressures and temperatures on the GSE/flight vehicle systems.

The GSE system will be upgraded for use with the pressure-fed 900 lbf thrust hybrid motor. Major changes to the system will include vacuum loading of propellants on-board the vehicle. For system simplification, the number of electrical quick-disconnect points will be reduced by the addition of on-board electronics. As mentioned earlier, a secondary external quick-disconnect line will need to be added for nitrogen pressurization. The current

system requires only two persons to man the GSE/launch operations. Fig. 9 shows a picture of the GSE hardware.

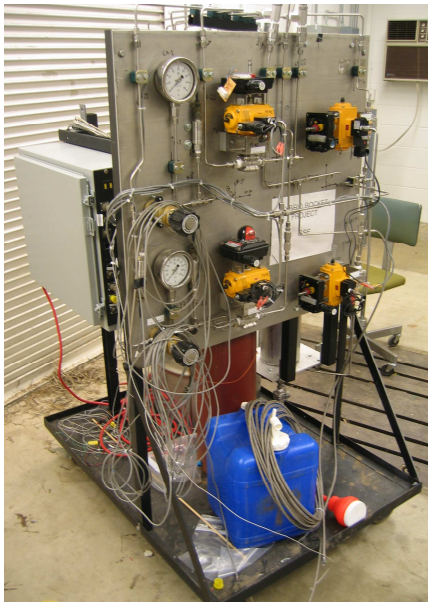

Figure 9. Picture of ground support equipment hardware.

LAUNCH OF RECOVERY SUB-SYSTEM

The incremental development of the technology demonstration hybrid rocket relies heavily on multiple launch and successful recovery of the flight hardware[4]. For this reason a robust and reliable parachute recovery system needs to be implemented. Following a recovery system trade study the final design calls for a dual deployment system, with drogue parachute deployment at apogee, and primary parachute deployment at 1,300 ft altitude. System redundancy is achieved by using two completely independent recovery modules for parachute ejection. Each module contains a lithium-ion battery, an R-DAS flight computer, and two pyrotechnic ejection charges (one for drogue and one for primary).

A series of ground tests were performed for the recovery system to ensure that avionics are functioning properly, and to determine the correct amount of 4F grade black powder that would be needed for successful parachute module pressurization and ejection. Too small of a pyrotechnic charge can result in ejection failure. Too large of a pyrotechnic charge can result in excessive separation forces being exerted on the recovery tethers potentially leading to structural failure of support joints and connectors. Ground tests showed that 6 grams of 4F grade black powder was an adequate charge for both drogue and primary parachute ejection.

The recovery sub-system consists of three modules as shown in Fig. A.2 in the appendix. The avionics module is located in between the drogue and primary parachute modules. The avionics module consists of a 6" diameter carbon-fiber coupler tube of 12" length. An internal aluminum chassis provides structural mounts and support for the following electronic devices: two R-DAS flight computers (for system redundancy), three 9V lithium-ion batteries, one 2-D accelerometer board, one valve relay board, one motion picture camera, as well as associated electrical wiring, d-sub connectors, mounting points, bolts, washers, etc. as shown in Fig. 10. The internal aluminum structure is secured to the outer carbon-fiber coupler via 4 threaded stainless-steel bolts and two bulkheads. The two plywood bulkheads are designed with water tight viton o-ring seals for water recovery. The dual redundant pyrotechnic charges are mounted on the external end of the bulkheads as shown in Fig. A.2.

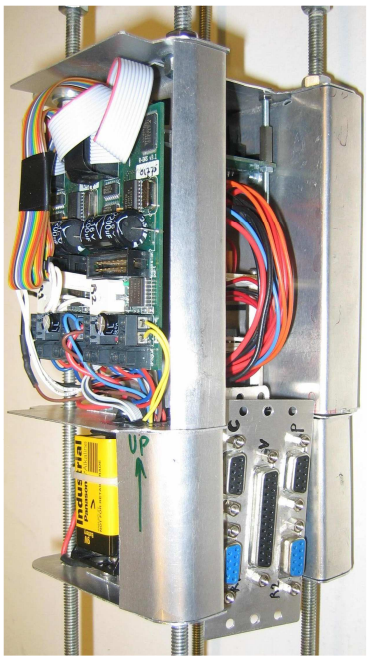

Figure 10. Picture of avionics hardware.

The drogue parachute module consists of a 6" diameter x 44.5" length carbon-fiber tube (0.08" thick) which contains the drogue parachute, 52 ft of nylon shock cord, 7 ft of kevlar shock cord, one piston assembly, one kevlar anti-zippering device, and associated stainless steel quicklink connectors. The drogue carbon-fiber tube is fastened to the avionics coupler via 4 expansion bolts. The drogue

parachute has 6.3 ft^2 of surface area and a tested Cd value of 1.16.

The primary parachute module consists of a 6" diameter x 47.9" length fiber-glass tube which contains the primary parachute, 76 ft of nylon shock cord, 7 ft of kevlar shock cord, one piston assembly, one kevlar anti-zippering device, and associated quicklink connectors. The primary parachute has 129 ft^2 of surface area, a tested Cd value of 2.92 and was sized to provide 15-25 ft/sec descent rates for the designed flight vehicle recovery mass. See schematic in Fig. A.2.

The recovery sub-system was launched on October 28, 2006 powered by an M-1900BB high-power solid rocket motor producing a maximum thrust of 520 lbf with a burn time of 3.23 seconds. The two onboard RDAS flight computers recorded an apogee of 4700 ft, an average of 7.7 G's during the thrust phase, and a maximum velocity of 610 ft/sec (Mach 0.53). Successful deployment of the drogue parachute occurred at t+18 sec (apogee), providing an instantaneous deceleration of 12 G's. Both pyrotechnic charges fired. Successful deployment of the main parachute occurred as planned, at an altitude of 1300 ft (t+87 sec), providing instantaneous deceleration of 31 G's. Both pyrotechnic charges fired. Vehicle soft landing occurred perfectly at t+145 sec. The successful launch and deployment of the recovery sub-system concluded the recovery testing phase. Figure 11 plots the RDAS flight data for velocity, altitude and acceleration versus time, noting the motor ignition, boost phase, motor burn-out, coasting phase, primary and drogue parachute deployment events.

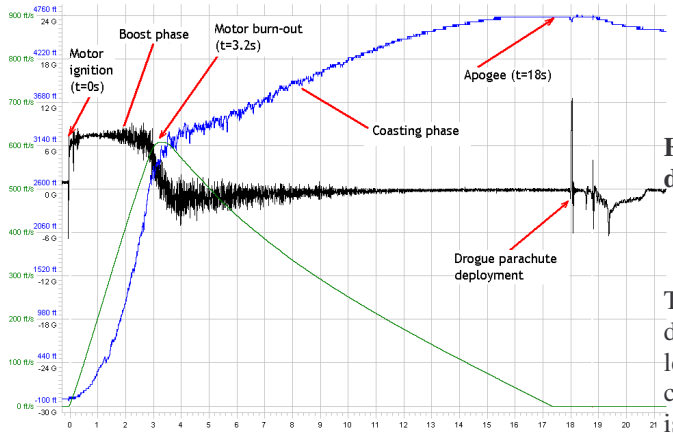

Figure 11. Plot of RDAS flight data for velocity (green), altitude (blue) and acceleration (black) versus time.

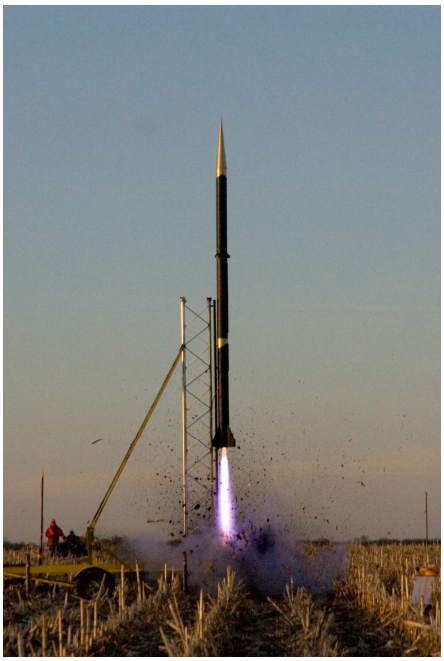

Figure 12. Launch of recovery sub-system qualification flight using a high-power solid rocket motor.

Figure 13. Successful deployment of primary and drogue parachutes.

FLIGHT VEHICLE DESIGN

The demonstration flight vehicle consists of a 6" diameter carbon-fiber aero-structure of three separate lengths which are assembled together with two carbon-fiber couplers. The total length of the vehicle is 18.5 ft or which 6.7 ft are taken by the avionics, primary and drogue parachute modules, and 8.5 ft consist of the oxidizer tank and propulsion modules as shown in Fig. 14. Four G10 fiberglass fins are bolted to the aft end with aluminum bracket mounts

providing a static stability margin of 7.6. The hybrid motor is secured to the vehicle via an aluminum thrust ring and rigid oxidizer feed lines. Upstream of the motor is the main solenoid valve, a quick-disconnect valve, and a temperature thermocouple. Further upstream, a 3.6 gallon hydrogen peroxide tank supplies the oxidizer. The forward end of the tank contains one pressure relief valve, one pressure transducer and one solenoid vent valve. The recovery sub-system is attached to the forward end of the oxidizer tank module through a 12" carbon-fiber coupler. The internal configuration of the flight vehicle is shown in Fig. 15. The vehicle gross lift of weight (GLOW) of 85.8 lb has the following mass breakdown: 9.8 lb H_2O_2 propellant/pressurant, 21.8 lb propulsion sub-system, 19.6 lb propellant feed sub-system, 25.3 lb recovery sub-system, and 9.3 lb aero-structure mass.

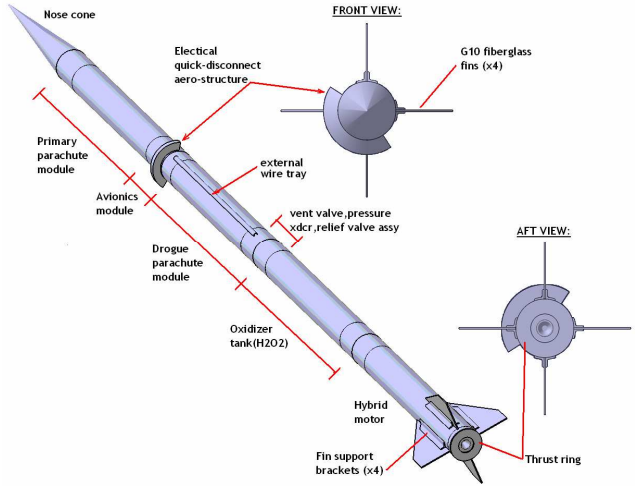

Figure 14. Schematic of demonstration flight vehicle.

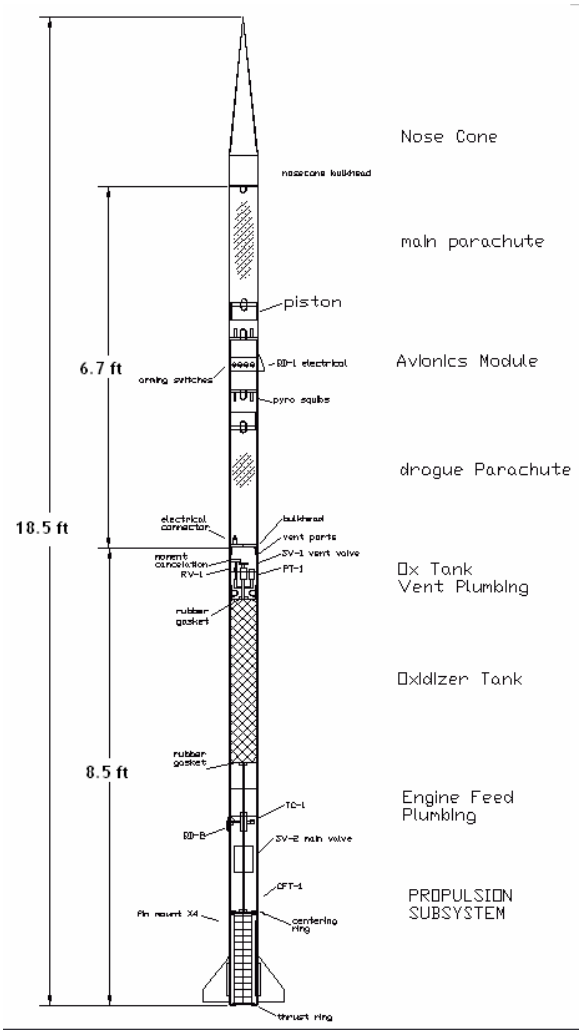

Figure 15. Flight vehicle internal configuration.

LIQUID INJECTION THRUST VECTOR CONTROL (LITVC)

The next step and quite possibly one of the most critical tasks in the program is to develop a guidance, navigation and control (GNC) system for the demonstration flight vehicle. The first step in that process was to decide on a control system strategy. The two primary candidates for thrust vector control of a hybrid rocket motor is an actuated flexible nozzle or a secondary injection system. The secondary injection system was chosen for its simplicity and ease of integration with the H_2O_2/LDPE hybrid motor. More specifically, a liquid injection thrust vector control (LITVC) system was selected due to the on-board availability of hydrogen peroxide. Thrust vectoring by liquid secondary injection is achieved by the injection of a fluid into the supersonic portion of the rocket nozzle. This injection produces a side force through a combination

of mechanisms. These mechanisms include the thrust of the jet itself, pressures on the nozzle wall from induced shock waves, and other various pressures on the wall caused from mass and energy addition into the rocket nozzle exhaust flow.[3] These effects, shown in Fig. 16, result in a net increase in pressure distributed over a portion of the nozzle wall in the vicinity of the injector. This unbalance of pressure over the circumference of the nozzle translates into a side force usable for thrust vectoring. The motor thrust is also augmented during vectoring by the axial component of the force produced from the increased pressures along the nozzle wall. This is in contrast to an actuated system in which axial thrust is reduced when thrust vectoring is engaged. LITVC is also an inherently rapid thrust vectoring mechanism with signal-to-force times of less than 20 milliseconds. This is a result of the low inertia of the mechanical systems that actuate the injectors.

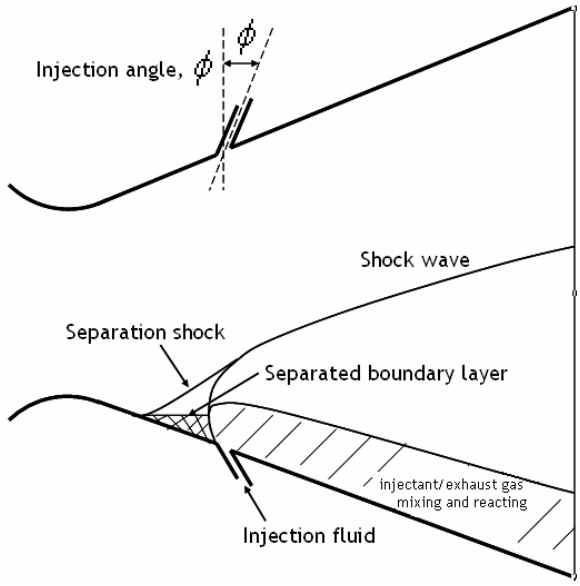

Figure 16. LITVC induced flow features

The LITVC system is particularly suited to the 900 lb_f thrust H_2O_2/LDPE hybrid motor since hydrogen peroxide is a reactive injectant. The decomposition of the hydrogen peroxide as well as its reaction with the exhaust products of the hybrid motor adds to the performance of the system. In order to design a flight weight LITVC system preliminary ground tests must be performed such that optimal operating conditions can be defined. This paper describes the design and development of the preliminary static ground test series for the hydrogen peroxide based LITVC system in which the effects of various parameters (i.e. flow rate, injection angle, etc.) are identified.

LITVC SYSTEM MODELING

In order to determine the system requirements for LITVC hardware the side force developed within the nozzle due to certain input conditions need to be well characterized. Mathematical models or historical data from similar systems can serve to predict these side forces and the overall performance of a particular design. Though some historical data for a hydrogen peroxide injectant exists, the information is limited in applicability, quantity, and availability. Any historical data will have to be extrapolated from test data for a solid or liquid propellant combination. This lack of applicable data along with the desire to produce application-specific test data is the primary motivation behind the proposed test series. This data will enable the student engineers to design higher fidelity and higher performance LITVC systems than what could previously be afforded for both the demonstrator rocket and the small launch vehicle.

The performance of an LITVC system can be characterized by the side specific impulse that it delivers. This side specific impulse can be separated into two sources; momentum and induced side specific impulse.

$$I_{sps} = \frac{F_s}{w} = I_{sps,m} + I_{sps,i} \qquad (1)$$

The momentum side specific impulse is what one would readily recognize as "Isp" as related to rocket performance. It is just the force produced by the momentum exchanged from the liquid jet to the nozzle wall. This is simply given as the average equivalent velocity, or injection velocity, over the standard acceleration of gravity at sea level. The injection velocity is given by the flow rate of the injectant divided by density and injection orifice area.

$$I_{sps,m} = \frac{V_i}{g_o} = \frac{4w}{\rho \pi d_i^2 g_o} \qquad (2)$$

The induced side specific impulse measures the performance due to the shock formation within the supersonic portion of the nozzle. The induced portion is the major contributor to the overall specific impulse of the system, usually producing over 95% of the side specific impulse. In order to model the side specific impulse we resort to an analytic approach that is calibrated with historical test data. James E. Broadwell first introduced this model in 1963 and it has since been adapted into industry.[1] This analysis, which is based upon blast wave theory, assumes injectant mixing and reaction with rocket

exhaust and allows for volume and drag effects. Broadwell's analysis is suited for our application since hydrogen peroxide is a reactive liquid that can produce large volumes of gas. The model is given below.

$$I_{sps,i} = C\sigma(\gamma_\infty)M_\infty V_\infty\left[1+\frac{1}{(\gamma_\infty-1)M_\infty^2}\frac{\rho_\infty}{\rho_i}\right]\frac{1}{g_o} \quad (3)$$

Here, M_∞, V_∞, ρ_∞, and γ_∞ are the free stream Mach number, velocity, density and specific heat ratio of the primary flow at the axial injection location. The function $\sigma(\gamma)$ is a function defined only by the free stream specific heat ratio and is determined via blast wave solutions in Broadwell's analysis. The function is modeled as a linear interpolation of two solutions, $\sigma(\gamma) = 0.35\gamma - 0.32$ since only two solutions in his analysis were given. The constant C included in the model, which is determined by experiment, is used to correct for approximations made in the analysis. Such approximations include the linearization of the system and the neglect of the boundary layer along the nozzle wall. Since this is a linear analysis, this constant adjusts the slope and magnitude of the prediction curve. Historical data for a 5,000 lb_f HP/Jet-A liquid-fueled rocket is available and suggests that the constant C used in Eq. 2 should be approximately 1.6.

The only currently undefined variable in Eq. 3 is ρ_i, defined as the density of the injectant after mixing and reacting occurs. This is a somewhat poorly defined variable but it is treated as follows.[1] The injectant is assumed to mix and react at constant pressure with a portion of the primary stream. This portion of the flow along with the injectant occupies a finite volume before mixing and reacting. After the reaction occurs the new products formed occupy a new finite volume. In general for hydrogen peroxide, this new volume is greater than the volume before the reaction since the decomposition of the liquid yields a large volume of gas products. Since the amount of injectant brings about this change in volume, the amount of injectant divided by the change in volume is set equal to ρ_i. The only issue with this calculation is that the amount of primary flow that actually mixes and reacts with the injectant is unknown.

However, this calculation can be performed for several injectant-to-primary mass flow rates in order to determine the practical range of ρ_i. By utilizing a thermochemestry code the pressure, temperature, and species of the exhaust gasses in the primary flow at the injection point can be computed. By listing all of the exhaust gas species as "fuel" and introducing the secondary injectant as an "oxidizer" one can specify a spectrum of "O/F" ratios in which the injectant and primary exhaust mix. Once again utilizing a thermochemistry code[2], constant pressure combustion of the fuel (exhaust gas species) and the oxidizer (injectant) can be carried out. Once the combustion has reached a new equilibrium the pressure and temperature of the mixture along with the mass in the system can be used to calculate the new volume via the perfect gas law. The initial volume is also computed from the perfect gas law; however, it uses the free stream pressure and temperature *before* the reaction. The volume contributed by the liquid injectant before the reaction can be computed from its density and the amount of mass injected. However, this liquid volume contributes negligibly to the overall computation and can usually be neglected.

Free stream density to injectant density ratio (ρ_∞/ρ_i) curves are provided in Fig. 17 for a H_2O_2/LDPE hybrid motor exhaust and several injectants. The results agree well with the results presented with Broadwell's analysis for a solid motor exhaust (90% H_2O_2 was not included in that analysis). Again, note that the injectant-to-primary ratio is *not* the injectant flow rate divided by the primary flow rate but rather the amount of injectant that mixes with a portion of the primary stream. From Fig. 17 one can see that the maximum and minimum values of the density ratio (ρ_∞/ρ_i) are approximately 1.7 and 0.5, respectively. Comparisons with historical data tend to show that the appropriate 'nominal' value should be set at the mean value of the bounds, or approximately ρ_∞/ρ_i =1.1.

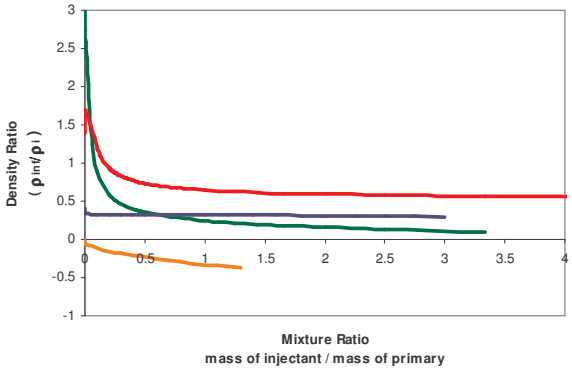

Figure 17. Density ratio as function of mixture ratio. *Results for a 400 psi chamber pressure 90% hydrogen peroxide / polyethelene hybrid motor exhaust. Injection location is at an area ratio of 2.4829. Injectants: LOx (green), 90% HP (red), Freon (blue), Water (yellow).*

LITVC SYSTEM REQUIREMENTS

The primary goal of this project is to produce reliable data such that a high fidelity LITVC system can be designed for an existing 900 lb_f thrust hybrid motor. The motor characteristics are summarized in Table 3a. A themochemestry code can be utilized to determine the free stream conditions at any length along the nozzle using the parameters listed in Table 3a. A very important design parameter is the axial distance along the nozzle in which injection occurs. Fortunately, this parameter is well defined from historical data. Typically, the best performance is obtained when the injector is located at a distance of 30% of the supersonic portion of the nozzle measured downstream from the throat (X/L = 0.3, where X is the axial length of the supersonic portion of the nozzle and L is the distance from the throat to the axial injection location). One would expect a maxima in performance to exist within the nozzle. As we move toward the throat, free stream conditions such as Mach number decrease, decreasing the performance of the system. Also, the shock tends to wrap around the nozzle wall, creating a small force in the direction opposite of the desired thrust vector, which degrades performance. As one moves the injection location toward the nozzle exit plane, performance increases from increase in Mach number. However, there is significantly less area in which the induced higher pressure region can act upon and less time for the injectant to mix and react with exhaust gasses. This once again causes performance to degrade.

Using the nozzle profile one can determine the area ratio at the desired injection point (X/L = 0.3). From this area ratio the free stream conditions can be computed via a thermochemestry code. These free stream conditions are listed in Table 3b. One can now predict the side forces developed for various flow rates once the injection velocity is determined. This velocity is only a function of injection flow rate and injection orifice diameter. It will be shown later that this diameter is of that listed in Table 3b. Given these parameters, a prediction curve for a single circular injection point normal to center line can be produced as in Fig. 18.

Now that the nominal case is defined as in Fig. 18 one can define specific flow rates to operate at. More specifically, one can define thrust vector angles to operate at and then determine the flow rate necessary to obtain that angle from the performance prediction curve. This is easily done since the arctangent of the ratio of side force to primary force is simply the thrust vector angle. Typical LITVC control systems operate up to 6º of thrust vector angle without incurring severe efficiency penalties. This limitation is imposed due to the fact that as flow rate is increased the shock grows and eventually wraps around the nozzle. This effect can be so dramatic as to create a maxima in which increasing flow rate beyond that value will cause the side force to decrease. This loss in performance at higher flow rates is illustrated in Fig. 18 by the dashed line. Because of this performance roll-off, only thrust vector angles up to six degrees will be tested.

Other characteristics that must be evaluated in an effort to maximize system performance and simulate integration issues are fluid injection angle, ablative nozzle erosion, slag buildup, and cosine losses due to more than one injection location being activated at the same instant. Injection angle affects both performance and nozzle erosion. The Broadwell analysis assumes a normal to centerline injection angle. Broadwell extended his analysis to include injection angle but the results were only satisfactory at best. Thus, the effects of injection angle will be included into the empirical constant, *C*. In general, performance increases as injection angle increases toward the throat up to approximately 20º. This increase in side force is due to the longer residence time of the injectant and the resulting stronger shock. However, this stronger shock also causes a more severe shock-surface interaction and local ablation rates, or nozzle erosion, is exacerbated. Nozzle erosion is also a relevant issue at a normal to centerline injection angle. The erosion problem can be abated by injecting downstream, which may be necessary if nozzle erosion is too severe at normal or upstream angles to be used in long duration applications.

Table 3. Rocket and injection parameters.
(a)Rocket parameters for the 900 lb_f hybrid motor.
(b)Properties at the LITVC injection point.

A	
Pc	400 psi
Oxidizer	90% H_20_2
Fuel	Polyethelene
Oxidizer Flow Rate	3.6 lb_f/s
O/F	7.5
Expansion Ratio	6.658
b	
Injection Area Ratio	2.4829
M∞	2.186
V∞	6809 ft/s
γ∞	1.1780
ρ∞	0.02075 lb/ft^3
d_{inj}	0.055 in

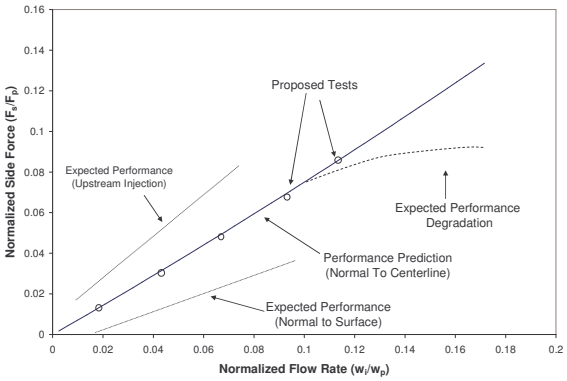

Figure 18. – Performance prediction. *The solid line is the performance prediction for a single orifice normal to centerline. Side force is normalized by the primary vacuum thrust. Injectant flow rate is normalized by primary flow rate.*

However, injecting downstream has been shown to reduce the performance of the system, as illustrated in Fig. 18. Testing at three representative angles (upstream, normal, and downstream) while observing nozzle erosion and performance levels should give some indication of an optimal system for a long duration motor.

Cosine losses are incurred when more than one orifice is activated. These losses are due to the overlapping of two or more shocks. The resultant force from the overlapping shocks will be less than the resultant force from the superposition of the individual shocks. These losses must be quantified for the 900 lb_f demonstration vehicle as well as for future LITVC designs for a small launch vehicle. Pressure ports will also be accommodated in the nozzle wall such that a future CFD analysis can be validated for single and dual orifice injections.

Finally, the least concerning design issue is slag plugging of the injection orifices. During the rocket firing, liquid silica from the silica phenolic wall can become lodged inside the injection orifice. Most data indicate that this is not a major concern, since the silica tends to stay in a liquid state during the burn and is easily evacuated once the injector is engaged. This can be easily tested by not engaging one injector until near the end of the firing. Inspection of the developed force will indicate any performance degradation.

The culmination of all the aforementioned testing parameters yields the testing matrix summarized in Table 4. Due to limited test stand availability and project funding only five tests can be performed, totaling approximately 50 seconds of burn time. Each test will be performed at a different flow rate in order to characterize the linear analysis model. Flow rates will correspond to 0.5º, 2º, 3.5º, 5º, and 6º of thrust vector angle. The 6º thrust vector angle will be used for a long duration burn in which all valves will be activated for the duration of the test. This will evaluate nozzle erosion characteristics for a worst-case scenario where the shock-surface interaction will be most severe. Multiple firings may be performed on the same nozzle as in Test #5 in a follow-on project to simulate a 50+ second burn time. Three injection angles will also be considered: normal to nozzle centerline, 20º upstream from nozzle centerline, and normal to local nozzle surface (downstream). There will be a total of four injectors, two of which will be aligned normal to centerline in order to validate cosine losses. All four injectors will be activated during each tested flow rate, resulting in three performance curves as illustrated in Fig. 18. Detailed transient response will be neglected in this investigation. This decision was made on the basis that more compact and faster acting injectors will be used on a flight vehicle, thus eliminating the relevance of transient response on a ‘work horse’ test rig. An illustrative steady state test sequence and layout is given in Fig. 19 a-b.

Table 4. Testing matrix summary. *Flow rates and developed side force necessary to obtain a desired thrust vector angle. All three injection angles will be tested during each test. Test 5 will activate all injectors for the duration of the burn. The reported side force is for the normal to centerline injection angle.*

	TVA (deg.)	Flow Rate (lb_f/s)	Side Force (lb_f)
Test 1	0.5	0.0498	7.9
Test 2	2	0.1954	31.4
Test 3	3.5	0.3359	55.0
Test 4	5	0.4719	78.7
Test 5*	6	0.5605	94.6

LITVC SYSTEM DESIGN

The LITVC system design is comprised of three main components: nozzle design and interface, injector and manifold design, and facility interfacing. Each component is designed to not only satisfy system requirements but to also try and reflect real-world conditions that will be seen in the demonstrator as well as a small launch vehicle application. This methodology allows for a "dry-run" design opportunity for a flight vehicle system. While not all elements will reflect a flight vehicle design in its entirety, this approach will paint a convincing picture of the integration feasibility of such a system.

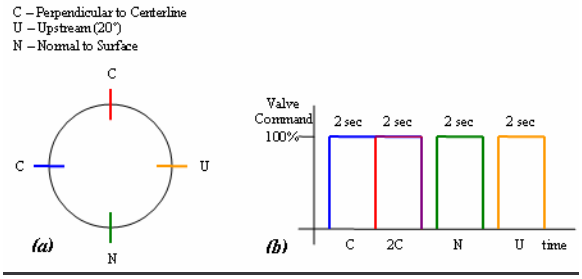

Figure 19. Injection location and testing sequence. *An illustrative example of the injection location and angles (a) as well as an illustrative testing sequence (b) for the liquid injection thrust vector control system. Note that (b) is not representative of test 5 in which all valves will be activated*

LITVC NOZZLE

The existing 900 lb_f H_2O_2/LDPE hybrid motor "work-horse", which was designed for other research endeavors at Purdue University, is a "battleship hardware" rocket with several unique features. This rocket utilizes a removable nozzle from a point just downstream of the existing throat location. The nozzle-chamber interface is a bolt-on flange that attaches the two components. The nozzle throat is also removable through the forward end of the motor as the existing design specifies a silica phenolic ablator throat. The throat is held in place by the phenolic chamber liner and an internal flange in the chamber.

Ideally, one would rather gain data that is readily applied to a small launch vehicle platform as well as the demonstrator rocket. In such an application, a contoured nozzle will most likely be used due to its lower divergence losses and consequent higher performance. However, due to a fixed skirt design, a fixed injection location and budgetary constraints a 13.5º conical nozzle was opted for. This conical nozzle was chosen in order to increase the thickness of the ablator near the exit plane of the nozzle. This was necessary since multiple tests will be performed on individual ablative nozzles due to financial constraints. The side force developed within the conical nozzle should agree very well with the side force developed in a contoured nozzle of an equivalent length. The ablative nozzle insert can be seen in Fig. 20.

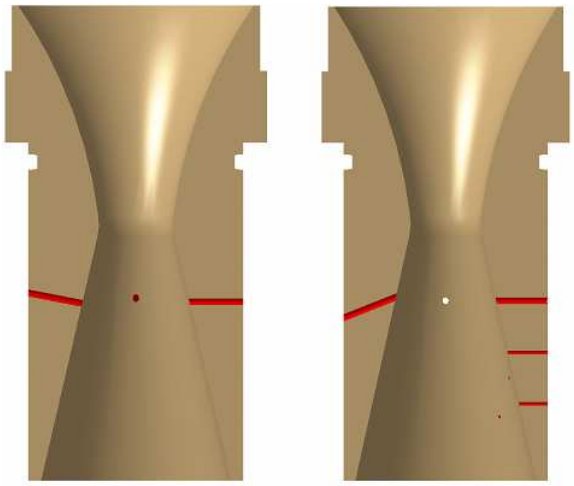

Figure 20. Ablative nozzle contour and injection ports. *The nozzle is a 13.5º conical nozzle. Two injection ports are at a normal-to-centerline angle. Two other ports are located at normal-to-surface and 20° upstream. Expansion Ratio: 6.658. Throat Diameter: 1.49 in.*

During the nozzle design process, many interfacing issues with the pre-existing hardware manifested itself. The first such issue was the injection point location. As previously discussed we would like to inject at thirty percent of the length of the diverging

portion of the nozzle, or X/L = 0.3. However, with the existing design that pointalong the nozzle would be located inside the combustion chamber casing. Since modification of the chamber is not an option the position of the throat had to be moved in the aft direction to accommodate the injection port. This effectively increased the volume of the aft mixing chamber, which should increase combustion efficiency of the hybrid motor. However, this gives the converging portion of the nozzle an overly exaggerated look, as shown in Fig. 20. The subsonic portion of the nozzle is contoured to allow for greater material thickness locally.

A removable one piece nozzle insert was chosen for this application. The single piece construction was selected to reduce failure modes consistent with sealing issues. Because the nozzle is a one piece design, the ablative insert is designed to install through the combustion chamber casing via the forward side of the motor. Since we are interested in measuring the nozzle erosion due to the shock-surface interaction a representative material that would be well suited in flight for a hybrid motor was chosen. Thus, a silica phenolic was selected for the application primarily because of its favorable regression rate and heritage at Purdue University.
A single nozzle skirt was designed to allow for testing of the four injection locations around the circumference of the nozzle and the three angles of injection. Two injector ports were dedicated to the normal to centerline injection angle and were separated by 90°. This was done in order to measure the cosine losses incurred when more than one injection orifice is activated. An injection port was also dedicated to the normal to surface (downstream) injection angle as well as the 20° upstream injection angle, all located at a separation angle of 90° for ease of integration. Pressure ports were also located near the two normal to centerline injection ports in order to collect pressure data along the nozzle wall when the injectors are engaged. The skirt will be constructed out of carbon steel and has female NPT threads to accommodate the injector and pressure transducer ports. The skirt bolts to the combustion chamber casing by way of a circular flange as shown in Fig. 1.

INJECTOR AND MANIFOLD

The injector architecture is based upon a simple fixed orifice design. This immediately reduces system complexity, schedule, and cost since servo valves and controllers are avoided. The on-off fixed orifice injector can provide various flow rates by simply adjusting the pressure upstream of the injector. Compact flight weight solenoid valves were first considered for use as injectors since they would most likely be installed on the demonstrator flight vehicle. However, due to the budgetary constraints of the project the solenoid valves were dropped in favor of less expensive pneumatically operated ball valves. Though the pneumatic ball valves are a bulkier choice, integration is not an issue on the test rig. This selection also allows for greater flexibility in attainable flow rates.

Given the desired flow rates in Table 4 we can determine our injection velocity by defining a convenient injection orifice diameter. Ideally one would like to replicate the injection velocity that the solenoid valve would induce. In theory, one attains enhanced performance from increasing the injection velocity by improving the momentum side specific impulse. However, the injection velocity must be reasonable so that head loss across the length of injection tube is not overwhelming. The solenoid valves have an injection orifice diameter of approximately 1/16 of an inch. A 1/8 in. (0.035 in. wall thickness) tube provides a comparable diameter of 0.055 in. and was selected for use downstream of the valve.

A trade study was performed in order to determine the injector and manifold configuration that would require the least amount of pressure head. The manifold was restricted to designs that produced very low flow velocities (<10 ft/s) in order to minimize any unnecessary pressure drop upstream of the injector and allow for even flow distribution. The study only considered off-the-shelf hardware in order to reduce manufacturing cost and lead time. The analysis found that the optimal configuration is that shown in Fig 21. The trend behind this configuration is to minimize the length of 1/8 inch (0.035 inch wall thickness) tubing. The velocities in the 1/8 inch tube at our maximum flow rates approach 400 ft/s – incurring a very substantial pressure drop over a very short length of tube.

The injector consists (from the manifold to the nozzle) of a ½ in. x ½ in. x ¼ in. reducing tee, a length of ¼ in. (0.035 in. wall thickness) tubing, a pneumatically operated ball valve (C_v = 0.6, ¼ in. tube connections), a second length of ¼ in. (0.035 in. wall thickness) tubing, a ¼ in. x 1/8 in. reducing union, and a final length of 1/8 in. (0.035 in. wall thickness) tubing. The 1/8 in. tubing will be secured to the nozzle skirt by a bored-through straight tube fitting with a male 1/8 in. NPT thread on the nozzle side and a Swagelok tube fitting on the injector side.

The 1/8 in. tube will be press fit into pre-drilled ports in the silica phenolic nozzle insert. This will provide an adequate seal between the exhaust gasses and the nozzle skirt. Preliminary thermal analysis indicates that the substantial amount of steel in the skirt and injector provides a large enough heat sink for the exposed injector tubes for the duration of the test. The silica phenolic ablation just downstream of the tube is thought to provide a cool cushion of gas to keep temperatures to a reasonable level. Also, the very act of injection is a means of cooling the exposed elements during a test.

The manifold is octagonal in shape and is constructed out of ½ in. (0.049 in. wall thickness) tubing. The manifold is fed by two opposite ½ in. tees from the facility in order to cancel out any momentum thrust that may be transferred to the test article; thus avoiding error in side force measurement. The ½ in. tubing was chosen to eliminate any unnecessary pressure drop across the injector as well as to improve distribution characteristics when more than one valve is activated at a time.

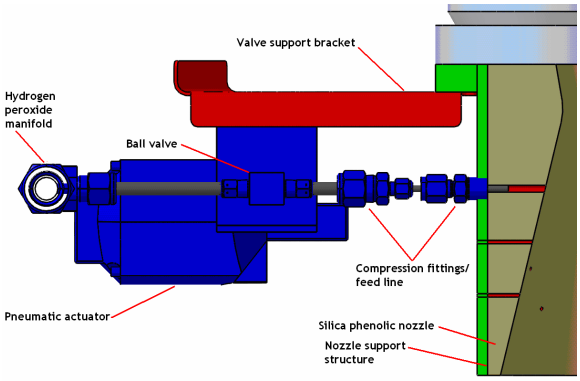

Figure 21. Injector layout

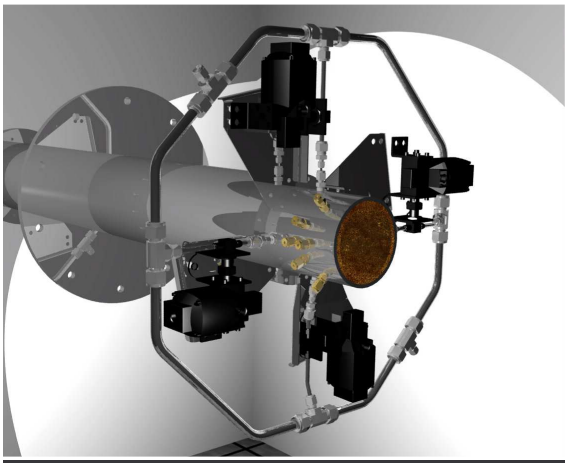

Figure 22. Hybrid motor, nozzle and manifold assembly.

As previously mentioned, the manifold feeds each injector through a ½ in. x ½ in. x ¼ in. reducing tee. The manifold is secured to the nozzle via the injectors in order to reduce any side force resistance provided through the tubing structure. Each injector is secured to the nozzle wall through a mounting bracket connected to the pneumatic actuator as seen in Fig. 22.

FACILITY

Given the flow rate requirements in Table 4 as well as the geometry of the manifold and injector the required facility interface pressure can be determined. The facility interface pressure is plotted as a function of required flow rate in Fig 23. Since this pressure varies significantly from the ullage pressure of the main oxidizer tank for the hybrid motor, a dedicated system will be needed to supply this pressure at the specified flow rates to the LITVC system. Luckily, a preexisting oxidizer tank and pressurant system is currently installed in the same test cell as the hybrid motor. The system utilizes a regulated gaseous nitrogen pressurization system with a vacuum H_2O_2 fill port. The complete system layout is shown in Fig. A.3 in the appendix.

Only minor modifications to the facility are needed. The fill/drain ports lines as well as the main line connecting the LITVC pressurization valve to the manifold interface needs to be installed as. This line will be constructed out of ½ in. (0.049 in. wall thickness) tubing in order to eliminate any unnecessary pressure drop across the facility line. Pressure drop calculations indicate that less than 10 psid of pressure drop will be seen across the facility main run lines for maximum anticipated flow rates. Based on this assessment, the facility interface pressure plot in Fig. 23 is a good indicator of required ullage pressure in the LITVC oxidizer tank. Therefore, tank ullage pressure is not expected to exceed 1,700 psi for any of the planned tests. This is well within structural limits as the maximum operating pressure of the tank is 5,000 psi. An expansion joint will be installed at the interface of the facility and the manifold in order to decouple the two components structurally. This is done to allow the manifold to move with the nozzle unabated when thrust vectoring is activated. This feature will help reduce the side force resistance due to facility structure and yield a more accurate side force measurement.

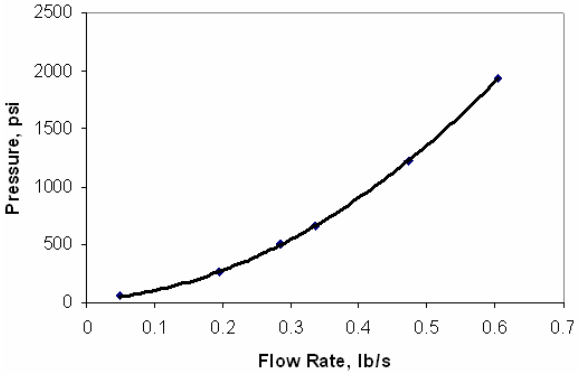

Figure 23. Facility interface required pressure

CONCLUSIONS

A hybrid rocket technology demonstrator is being designed and tested at Purdue University, to serve as a test-bed for flight testing technologies critical to the development of a small satellite launch vehicle capable of delivering a 10 lb payload to Low Earth Orbit. To date, significant progress has been made on the hybrid rocket technology demonstrator. Based on the design of the 250 lbf hybrid rocket motor, a more powerful, 4-port 900 lbf thrust hybrid motor has been designed and successfully hot fire tested at Purdue University rocket test facilities. This motor will serve to flight test the demonstrator vehicle LITVC and GNC systems in the near future. In addition, the ground support equipment for remote launch operations has been designed and manufactured. Also, the recovery sub-system was successfully ground and flight tested on a solid rocket booster.

Data gained from the hydrogen peroxide based LITVC system for the 900 lb_f H_2O_2/LDPE hybrid motor will enable student engineers at Purdue University to design higher fidelity and higher performance LITVC systems than what could previously be afforded for the demonstrator rocket flight vehicle as well as the small launch vehicle. The test series will characterize a number of parameters in relation to the side force developed within the nozzle as well as in relation to the physical behavior of the system. These parameters include injection flow rate, injection angle, nozzle erosion, slag plugging and cosine losses. Facility build-up and test article integration is currently underway. Testing is to commence immediately following the completion of the facility and test article integration.

ACKNOWLEDGEMENTS

The authors would like to thank the members of the Purdue University Hybrid Rocket Project team, as well as Scott Meyer for their help and support. We would also like to acknowledge the sponsors to the Hybrid Rocket project and thank them for their support: Purdue Engineering Student Council and Purdue School of Aeronautics and Astronautics.

REFERENCES

[1]Broadwell, J., "Analysis of the Fluid Mechanics of Secondary Injection for Thrust Vector Control," *AIAA Journal*, Vol. 1, No. 5, 1963, pp 1067-1075.

[2]Gordon, S., McBride, B, *Computer Program for Calculation of Complex Chemical Equilibrium Compositions, Rocket Performance, Incident and Reflected Shocks, and Chapman-Jouguet Detonations*, NASA SP-273, 1971.

[3]NASA SP-8114, "Solid Rocket Thrust Vector Control," *NASA Space Vehicle Design Criteria (Chemical)*, NASA Lewis Research Center (Cleveland, OH), December, 1974.

[4]Tsohas, J., Droppers, L., Heister, S.,"Sounding Rockt Technology Demonstrator for Small Satellite Launch Vehicle Project," AIAA-RS4 2006-4004.

[5]Vonderwell, D., Murray, I., Heister, S., "Optimization of Hybrid Rocket Booster Fuel Grain Design," *Journal of Spacecraft and Rockets*, Vol. 32. No 6, November-December 1995, pp 964-969.

APPENDIX

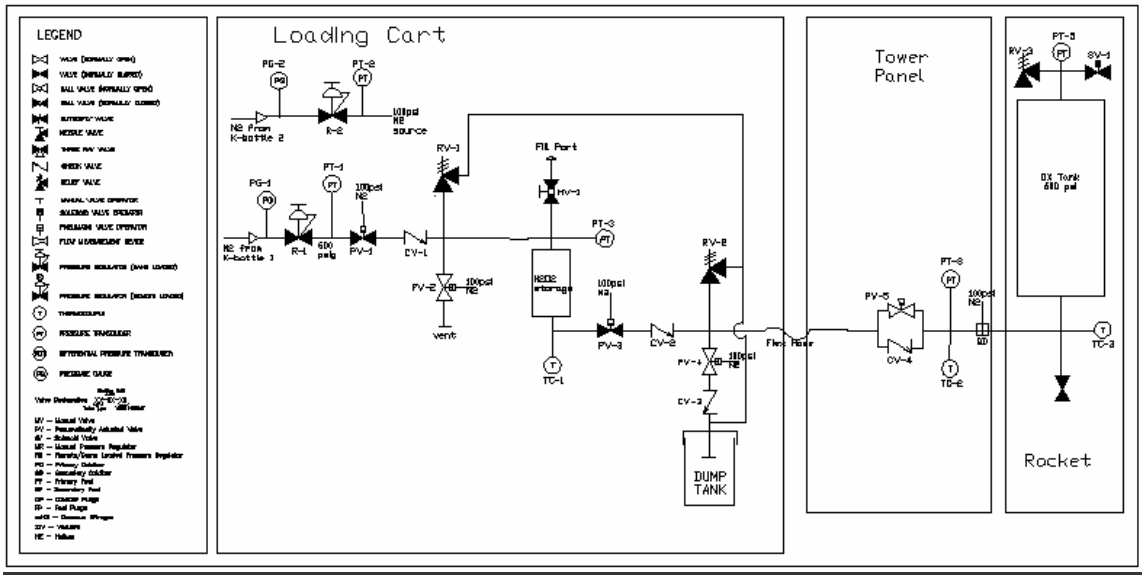

Figure A.1. Ground support equipment plumbing and instrumentation diagram

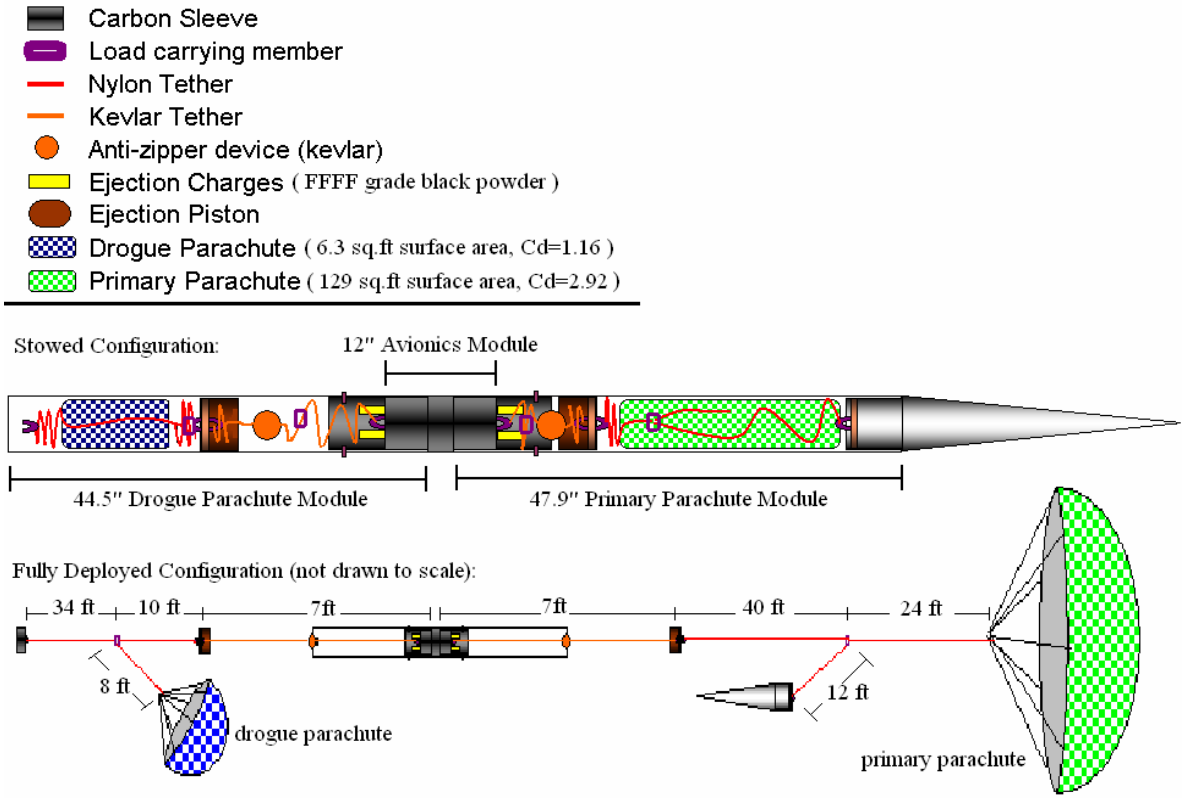

Figure A.2. Recovery sub-system layout

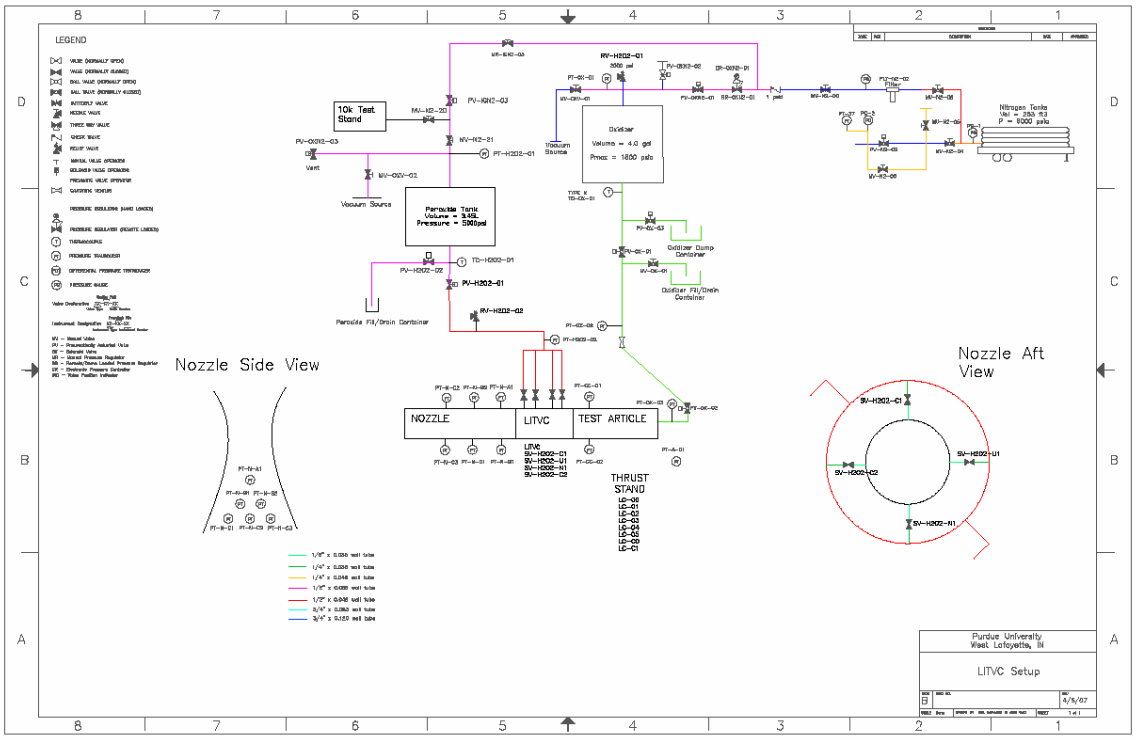

Figure A.3. LITVC Facility Plumbing and Instrument Diagram (P&ID)